3458 *Chem. Mater.* **2009,** *21,* 3458–3468
DOI:10.1021/cm901033m

CHEMISTRY OF MATERIALS
Article

Formation Mechanism and Shape Control of Monodisperse Magnetic $CoFe_2O_4$ Nanocrystals

Ningzhong Bao,*[,†] Liming Shen,[†] Wei An,[‡] Prahallad Padhan,[†] C. Heath Turner,[‡] and Arunava Gupta*[,†]

[†]*Center for Materials for Information Technology and* [‡]*Department of Chemical and Biological Engineering, University of Alabama, Tuscaloosa, Alabama 35487*

Received April 14, 2009

The formation mechanism and shape control of monodisperse magnetic cobalt ferrite ($CoFe_2O_4$) nanocrystals produced by thermolysis of a stoichiometric $Co^{2+}Fe_2^{3+}$−oleate complex in organic solution has been investigated. Synthesis of the pure ternary $CoFe_2O_4$ inverse spinel phase, without formation of any intermediate binary cobalt and iron oxides, is favored by the close thermal decomposition temperature of the Co^{2+}−oleate and Fe^{3+}−oleate precursors. For reaction temperatures between 250 and 320 °C, the nucleation and growth dynamics dictate the size and shape evolution of the nanocrystals. Prenucleation of $CoFe_2O_4$ occurs at 250−300 °C but without any growth of nanocrystals, because the monomer concentration is lower than the critical nucleation concentration. For temperatures in the range of 300−320 °C, which is above the thermolysis temperature of the mixed $Co^{2+}Fe_2^{3+}$−oleate complex, the monomer concentration increases rapidly resulting in homogeneous nucleation. Atomic clusters of $CoFe_2O_4$ with size <2 nm are initially formed at 314 °C that then grow rapidly when the temperature is raised to 320 °C in less than a minute. The shape of the $CoFe_2O_4$ nanocrystals can be reproducibly controlled by prolonging the aging time at 320 °C, evolving from initial spherical, to spherical-to-cubic, cubic, corner-grown cubic, or starlike shapes. Thus, with careful choice of reaction parameters, such as the precursor concentration and the heating rate, it is possible to achieve large-scale synthesis of shape-controlled monodisperse $CoFe_2O_4$ nanocrystals with high yield.

Introduction

Nanocrystals have received considerable interest because of their fascinating shape- and size-dependent properties, not only for fundamental scientific research but also for a wide range of technological applications.[1] The ability to control the size, shape, composition, monodispersity, and surface properties of the nanocrystals is critically important for studying their intrinsic properties and for exploiting their novel optical, electric, and magnetic properties for practical applications.[2] The past two decades have seen impressive advances in the tailored synthesis of monodisperse nanocrystals with uniform size, shape, and composition.[1,2] Monodisperse nanocrystals of a wide variety of materials, including metals,[3] oxides,[4] chalcogenides,[5] and others,[6] have been successfully synthesized using different methods such as hydrothermal/solvothermal,[7] nonhydrolytic,[2a,5a,8] and thermal decomposition[3−6] routes. Among chemical methods, thermal decomposition of organometallic compounds in high-boiling-point inert organic solvents has proven to be an attractive route for the synthesis of monodisperse nanocrystals with high yield, narrow size distribution, and good crystallinity.[3−6]

An improved understanding of the synthetic mechanism is important for the controllable synthesis of monodisperse nanocrystals of different shapes and sizes.

*Corresponding author. E-mail: nzhbao@mint.ua.edu (N.B.); agupta@mint.ua.edu (A.G.).

(1) (a) Peng, X. *Adv. Mater.* **2003**, *15*, 459. (b) Hyeon, T. *Chem. Commun.* **2003**, 927. (c) Xia, Y.; Yang, P.; Sun, Y.; Wu, Y.; Mayers, B.; Gates, B.; Yin, Y.; Kim, F.; Yan, H. *Adv. Mater.* **2003**, *15*, 353. (d) Yin, Y.; Alivisatos, A. P. *Nature* **2005**, *437*, 664. (e) Jun, Y. W.; Choi, J. S.; Cheon, J. *Angew. Chem., Int. Ed.* **2006**, *45*, 3414. (f) Sun, S. *Adv. Mater.* **2006**, *18*, 393. (g) Park, J.; Joo, J.; Kwon, S. G.; Jang, Y.; Hyeon, T. *Angew. Chem., Int. Ed.* **2007**, *46*, 4630. (h) Xia, Y.; Xiong, Y.; Lim, B.; Skrabalak, S. E. *Angew. Chem., Int. Ed.* **2009**, *48*, 60.

(2) (a) Brus, L. E. *J. Chem. Phys.* **1984**, *80*, 4403. (b) Steigerwald, M. L.; Brus, E. *Acc. Chem. Res.* **1990**, *23*, 183. (c) Alivisatos, A. P. *Science* **1996**, *271*, 933. (d) Li, L.; Hu, J.; Yang, W.; Alivisatos, A. P. *Nano Lett.* **2001**, *1*, 349. (e) El-Sayed, M. A. *Acc. Chem. Res.* **2004**, *37*, 326. (f) Hu, J.; Li, L.; Yang, W.; Manna, L.; Wang, L.; Alivisatos, A. P. *Science* **2001**, *292*, 2060. (g) Wang, X.; Peng, Q.; Li, Y. *Acc. Chem. Res.* **2007**, *40*, 635.

(3) (a) Sun, S.; Murray, C. B.; Weller, D.; Folks, L.; Moser, A. *Science* **2000**, *287*, 1989. (b) Sun, S.; Anders, S.; Hamann, H. F.; Thiele, J. U.; Baglin, J. E. E.; Thomson, T.; Fullerton, E. E.; Murray, C. B.; Terris, B. D. *J. Am. Chem. Soc.* **2002**, *124*, 2884. (c) Chen, M.; Liu, J. P.; Sun, S. *J. Am. Chem. Soc.* **2004**, *126*, 8394. (d) Peng, S.; Wang, C.; Xie, J.; Sun, S. *J. Am. Chem. Soc.* **2006**, *128*, 10676. (e) Chen, M.; Kim, J.; Liu, J. P.; Fan, H.; Sun, S. *J. Am. Chem. Soc.* **2006**, *128*, 7132. (f) Wang, C.; Hou, Y.; Kim, J.; Sun, S. *Angew. Chem., Int. Ed.* **2007**, *46*, 6333. (g) Wang, C.; Daimon, H.; Onodera, T.; Koda, T.; Sun, S. *Angew. Chem., Int. Ed.* **2008**, *47*, 3588. (h) Jana, N. R.; Peng, X. *J. Am. Chem. Soc.* **2003**, *125*, 14280. (i) Ji, X.; Song, X.; Li, J.; Bai, Y.; Yang, W.; Peng, X. *J. Am. Chem. Soc.* **2007**, *129*, 13939. (j) Son, S. U.; Jang, Y.; Yoon, K. Y.; Kang, E.; Hyeon, T. *Nano Lett.* **2004**, *4*, 1147. (k) Kim, J.; Park, S.; Lee, J. E.; Jin, S. M.; Lee, J. H.; Lee, I. S.; Yang, I.; Kim, J. S.; Kim, S. K.; Cho, M. H.; Hyeon, T. *Angew. Chem., Int. Ed.* **2006**, *45*, 7754.

Published on Web 06/12/2009

Although there are numerous reports on synthesis, the investigation of the formation mechanism and related shape control of uniform nanocrystals is rather limited, in particular for multicomponent systems.[1,9] Mechanistic studies of the thermal decomposition method indicate that both heterogeneous and homogeneous nucleation followed by growth can lead to the formation of monodisperse nanocrystals.[1,10] For heterogeneous nucleation and growth, the seeded-growth technique is effective in providing both single-phase and heterostructured nanocrystals, such as core−shell structure, etc., with good size control.[11] Here, the uniformity of the initial nanocrystal seeds determines the monodispersity and uniformity of the final product. Thermolysis of precursors in a high-boiling-point solvent can also result in the controlled synthesis of monodisperse nanocrystals. This involves a burst of homogeneous nucleation followed by a diffusion-controlled growth process.[1,12] Both the injection of reactants into a hot solvent, and the thermolysis of reactants premixed with the solvent, can help control the degree of supersaturation as well as the monomer concentration in order to accomplish homogeneous nucleation separated from the growth process.[1,13] The former method produces a high degree of supersaturation by the rapid injection of excess precursor into a hot surfactant solution, resulting in a nucleation burst. Similarly, the latter provides a suitable condition for supersaturation by careful control of the process conditions, such as the heating rate and the reactant concentrations.[1,10]

The inverse spinel ferrites of ternary composition MFe_2O_4 (M = Co, Ni, Mn, Fe, etc.) constitute an important class of insulating magnetic materials that are widely used for applications in microwave and information storage devices, biotechnology/biomedicine, and environmental remediation.[14] In general, the chemical

(4) (a) Urban, J. J.; Yun, W. S.; Gu, Q.; Park, H. *J. Am. Chem. Soc.* **2002**, *124*, 1186. (b) Jun, Y.; Casula, M. F.; Sim, J. H.; Kim, S. Y.; Cheon, J.; Alivisatos, A. P. *J. Am. Chem. Soc.* **2003**, *125*, 15981. (c) Cozzoli, P. D.; Kornowski, A.; Weller, H. *J. Am. Chem. Soc.* **2003**, *125*, 14539. (d) Yin, M.; Gu, Y.; Kuskovsky, I. L.; Andelman, T.; Zhu, Y.; Neumark, G. F.; O'Brien, S. *J. Am. Chem. Soc.* **2004**, *126*, 6206. (e) Jana, N. R.; Chen, Y.; Peng, X. *Chem. Mater.* **2004**, *16*, 3931. (f) Chen, Y.; Kim, M.; Lian, G.; Johnson, M. B.; Peng, X. *J. Am. Chem. Soc.* **2005**, *127*, 13331. (g) Narayanaswamy, A.; Xu, H.; Pradhan, N.; Peng, X. *Angew. Chem., Int. Ed.* **2006**, *45*, 5361. (h) Narayanaswamy, A.; Xu, H.; Pradhan, N.; Kim, M.; Peng, X. *J. Am. Chem. Soc.* **2006**, *128*, 10310. (i) Chen, Y.; Johnson, E.; Peng, X. *J. Am. Chem. Soc.* **2007**, *129*, 10937. (j) Hou, Y.; Xu, Z.; Sun, S. *Angew. Chem., Int. Ed.* **2007**, *46*, 6329. (k) Peng, S.; Sun, S. *Angew. Chem., Int. Ed.* **2007**, *46*, 4155. (l) Lee, K.; Seo, W. S.; Park, J. T. *J. Am. Chem. Soc.* **2003**, *125*, 3408. (m) Joo, J.; Yu, T.; Kim, Y. W.; Park, H. M.; Wu, F.; Zhang, J. Z.; Hyeon, T. *J. Am. Chem. Soc.* **2003**, *125*, 6553. (n) Yu, T.; Joo, J.; Park, Y.; Hyeon, T. *Angew. Chem., Int. Ed.* **2005**, *44*, 7411. (o) Park, J.; Lee, E.; Hwang, N. M.; Kang, M.; Kim, S. C.; Hwang, Y.; Park, J. G.; Noh, H. J.; Kim, J. Y.; Park, J. H.; Hyeon, T. *Angew. Chem., Int. Ed.* **2005**, *44*, 2872. (p) Kim, D.; Park, J.; An, K.; Yang, N. K.; Park, J. G.; Hyeon, T. *J. Am. Chem. Soc.* **2007**, *129*, 5812. (q) Pacholski, C.; Kornowski, A.; Weller, H. *Angew. Chem., Int. Ed.* **2002**, *41*, 1188.

(5) (a) Murray, C. B.; Norris, D. J.; Bawendi, M. G. *J. Am. Chem. Soc.* **1993**, *115*, 8706. (b) Peng, X.; Schlamp, M. C.; Kadavanich, A. V.; Alivisatos, A. P. *J. Am. Chem. Soc.* **1997**, *119*, 7019. (c) Chen, C. C.; Herhold, A. B.; Johnson, C. S.; Alivisatos, A. P. *Science* **1997**, *276*, 398. (d) Manna, L.; Scher, E. C.; Alivisatos, A. P. *J. Am. Chem. Soc.* **2000**, *122*, 12700. (e) Peng, Z. A.; Peng, X. *J. Am. Chem. Soc.* **2001**, *123*, 183. (f) Peng, Z. A.; Peng, X. *J. Am. Chem. Soc.* **2001**, *123*, 1389. (g) Yu, W. W.; Peng, X. *Angew. Chem., Int. Ed.* **2002**, *41*, 2368. (h) Yu, W. W.; Wang, Y. A.; Peng, X. *Chem. Mater.* **2003**, *15*, 4300. (i) Pradhan, N.; Peng, X. *J. Am. Chem. Soc.* **2007**, *129*, 3339. (j) Peng, X.; Manna, L.; Yang, W.; Wickham, J.; Scher, E.; Kadavanich, A.; Alivisatos, A. P. *Nature* **2000**, *404*, 59. (k) Pradhan, N.; Reifsnyder, D.; Xie, R.; Aldana, J.; Peng, X. *J. Am. Chem. Soc.* **2007**, *129*, 9500. (l) Joo, J.; Na, H. B.; Yu, T.; Yu, J. H.; Kim, Y. W.; Wu, F.; Zhang, J. Z.; Hyeon, T. *J. Am. Chem. Soc.* **2003**, *125*, 11100. (m) Jun, Y.; Lee, S. M.; Kang, N. J.; Cheon, J. *J. Am. Chem. Soc.* **2001**, *123*, 5150. (n) Jun, Y.; Jung, Y.; Cheon, J. *J. Am. Chem. Soc.* **2002**, *124*, 615. (o) Lee, S. M.; Jun, Y. W.; Cho, S. N.; Cheon, J. *J. Am. Chem. Soc.* **2002**, *124*, 11244. (p) Manna, L.; Scher, E. C.; Alivisatos, A. P. *J. Am. Chem. Soc.* **2000**, *122*, 12700. (q) Manna, L.; Milliron, D. J.; Meisel, A.; Scher, E. C.; Alivisatos, A. P. *Nat. Mater.* **2003**, *2*, 382. (r) Milliron, D. J.; Hughes, S. M.; Cui, Y.; Manna, L.; Li, J.; Wang, L. W.; Alivisatos, A. P. *Nature* **2004**, *430*, 190. (s) Zhong, X.; Feng, Y.; Knoll, W.; Han, M. *J. Am. Chem. Soc.* **2003**, *125*, 13559. (t) Sigman, M. B.; Ghezelbash, A.; Hanrath, T.; Sauders, A. E.; Lee, F.; Korgel, B. A. *J. Am. Chem. Soc.* **2003**, *125*, 16050. (u) Si, R.; Zhang, Y. W.; You, L. P.; Yan, C. H. *Angew. Chem., Int. Ed.* **2005**, *44*, 3256.

(6) (a) Park, J.; Koo, B.; Hwang, Y.; Bae, C.; An, K.; Park, J. G.; Park, H. M.; Hyeon, T. *Angew. Chem., Int. Ed.* **2004**, *43*, 2282. (b) Park, J.; Koo, B.; Yoon, K. Y.; Hwang, Y.; Kang, M.; Park, J. G.; Hyeon, T. *J. Am. Chem. Soc.* **2005**, *127*, 8433. (c) Kim, Y. H.; Jun, Y.; Jun, B. H.; Lee, S. M.; Cheon, J. *J. Am. Chem. Soc.* **2002**, *124*, 12656. (d) Qian, C.; Kim, F.; Ma, L.; Tsui, F.; Yang, P.; Liu, J. *J. Am. Chem. Soc.* **2004**, *126*, 1195. (e) Li, Y.; Malik, M. A.; O'Brien, P. *J. Am. Chem. Soc.* **2005**, *127*, 16020.

(7) Wang, X.; Zhuang, J.; Peng, Q.; Li, Y. *Nature* **2006**, *437*, 121.

(8) (a) Vioux, A. *Chem. Mater.* **1997**, *9*, 2292. (b) Trentler, T. J.; Denler, T. E.; Bertone, J. F.; Agrawal, A.; Colvin, V. L. *J. Am. Chem. Soc.* **1999**, *121*, 1613. (c) Puntes, V. F.; Krishnan, K. M.; Alivisatos, A. P. *Science* **2001**, *291*, 2115. (d) Yin, M.; OLBrien, S. *J. Am. Chem. Soc.* **2003**, *125*, 10180. (e) Hyeon, T.; Lee, S. S.; Park, J.; Chung, Y.; Na, H. B. *J. Am. Chem. Soc.* **2001**, *123*, 12798.

(9) (a) Oxtoby, D. W. *Nature* **2000**, *406*, 464. (b) Auer, S.; Frenkel, D. *Nature* **2001**, *409*, 1020. (c) Gasser, U.; Weeks, E. R.; Schofield, A.; Pusey, P. N.; Weitz, D. A. *Science* **2001**, *292*, 258. (d) Bullen, C. R.; Mulvaney, P. *Nano Lett.* **2004**, *4*, 2303. (e) Asokan, S.; Krueger, K. M.; Alkhawaldeh, A.; Carreon, A. R.; Mu, Z.; Colvin, V. L.; Mantzaris, N. V.; Wong, M. S. *Nanotechnology* **2005**, *16*, 2000. (f) Embden, J.; Mulvaney, P. *Langmuir* **2005**, *21*, 10226. (g) Winkler, P. M.; Steiner, G.; Vrtala, A.; Vehkamäki, H.; Noppel, M.; Lehtinen, K. E. J.; Reischl, G. P.; Wagner, P. E.; Kulmala, M. *Science* **2008**, *319*, 1374.

(10) (a) Peng, X.; Wickham, J.; Alivisatos, A. P. *J. Am. Chem. Soc.* **1998**, *120*, 5343. (b) Peng, Z. A.; Peng, X. *J. Am. Chem. Soc.* **2002**, *124*, 3343. (c) De Smet, Y.; Deriemaeker, L.; Finsy, R. *Langmuir* **1997**, *13*, 6884. (d) Wilcoxon, J. P.; Provencio, P. P. *J. Am. Chem. Soc.* **2004**, *126*, 6402. (e) Yu, H.; Gibbons, P. C.; Kelton, K. F.; Buhro, W. E. *J. Am. Chem. Soc.* **2001**, *123*, 9198. (f) Zhou, X. J.; Huebner, W.; Anderson, H. V. *Appl. Phys. Lett.* **2002**, *80*, 3814.

(11) (a) Li, J. J.; Wang, Y. A.; Guo, W.; Keay, J. C.; Mishima, T. D.; Johnson, M. B.; Peng, X. *J. Am. Chem. Soc.* **2003**, *125*, 12567. (b) Guo, W.; Li, J. J.; Wang, Y. A.; Peng, X. *J. Am. Chem. Soc.* **2003**, *125*, 3901. (c) Battaglia, D.; Blackman, B.; Peng, X. *J. Am. Chem. Soc.* **2005**, *127*, 10889. (d) Zeng, H.; Li, J.; Wang, Z. L.; Liu, J. P.; Sun, S. *Nano Lett.* **2004**, *4*, 187. (e) Yu, H.; Chen, M.; Rice P. M.; Wang, S. X.; White, R. L.; Sun, S. *Nano Lett.* **2005**, *5*, 379. (f) Li, Y.; Zhang, Q.; Nurmikko, A. V.; Sun, S. *Nano Lett.* **2005**, *5*, 1689. (g) Xu, C.; Xie, J.; Ho, D.; Wang, C.; Kohler, N.; Walsh, E. G.; Morgan, J. R.; Chin, Y. E.; Sun, S. *Angew. Chem., Int. Ed.* **2008**, *47*, 173. (h) Gu, H.; Zheng, R.; Zhang, X.; Xu, B. *J. Am. Chem. Soc.* **2004**, *126*, 5664. (i) Mokari, T.; Tothenberg, E.; Popov, I.; Costi, R.; Banin, U. *Science* **2004**, *304*, 1787. (j) Mokari, T.; Sztrum, C. G.; Salant, A.; Rabani, E.; Banin, U. *Nat. Mater.* **2005**, *4*, 855.

(12) (a) Xu, Z.; Hou, Y.; Sun, S. *J. Am. Chem. Soc.* **2007**, *129*, 8698. (b) Choi, S. H.; Na, H. B.; Park, Y. I.; An, K.; Kwon, S. G.; Jang, Y.; Park, M.; Moon, J.; Son, J. S.; Song, I. C.; Moon, W. K.; Hyeon, T. *J. Am. Chem. Soc.* **2008**, *130*, 15573.

(13) (a) Vossmeyer, T.; Katsikas, L.; Giersig, M.; Popovic, I. G.; Diesner, K.; Chemseddine, A.; EychmUller, A.; Weller, J. H. *J. Phys. Chem.* **1994**, *98*, 7665. (b) Spanhel, L.; Anderson, M. A. *J. Am. Chem. Soc.* **1991**, *113*, 2826.

(14) (a) Raj, K.; Moskowitz, R. *J. Magn. Magn. Mater.* **1990**, *85*, 233. (b) Sugimoto, M. *J. Am. Ceram. Soc.* **1999**, *82*, 269. (c) Smit, J.; Wijn, H. P. J. Ferrites; Wiley: New York, 1959. (d) O'Handley, R. C. Modern Magnetic Materials−Principles and Applications; John Wiley & Sons: New York, 2000. (e) Sun, S.; Zeng, H.; Robinson, D. B.; Raoux, S.; Rice, P. M.; Wang, S. X.; Li, G. J. Am. Chem. Soc. 2004, 126, 273.

composition, structure, size, and shape determine the performance of a magnetic material.[16] For example, the switching properties of nanostructured magnetic materials are sensitive to the geometric shape due to the dominating role of shape anisotropy in magnetism.[16] Similarly, when the size is below a critical value (typically less than 10 nm), the individual nanoparticles behave as a single magnetic domain, exhibiting superparamagnetic behavior above the so-called blocking temperature.[17] The individual nanoparticles possess a large magnetic moment, but because of thermal activation behave like a giant paramagnetic atom. They respond rapidly to an applied magnetic field, but exhibit negligible remanence (residual magnetism) and coercivity (the field required to bring the magnetization to zero). These features make superparamagnetic nanoparticles attractive for a broad range of biomedical applications, primarily because agglomeration resulting from strong magnetic interaction is avoided.[18] Cobalt ferrite ($CoFe_2O_4$), one of the most intensively investigated ferrites because of its large magnetocrystalline anisotropy, has successfully been synthesized in the form of monodisperse cubic and spherical nanoparticles by the seed-mediated growth process using $Fe(acac)_3$ and $Co(acac)_2$ as reactants.[16a,16b,19] We recently reported on the synthesis of monodisperse ferrite nanocrystals by controlled thermolysis of a precursor consisting of mixed metal oleates.[20] A more detailed investigation of the formation mechanism of monodisperse ferrite nanocrystals is desirable because the findings are likely relevant for the synthesis of other multicomponent systems, in particular for shape control.

In this paper, we present a systematic study of the formation mechanism and shape control of monodisperse $CoFe_2O_4$ nanocrystals formed by thermolysis of a homogeneous mixture of iron and cobalt oleates. We have explored the correlation of the thermal decomposition behavior with the structure of the precursor, both based on theoretical calculations and thermogravimetric analysis. We have further investigated in detail the reaction temperature- and reaction time-dependent shape, size, and magnetization changes of the product. A better understanding of the formation mechanism has enabled us to reproducibly control the shape of the nanocrystals in the form of spherical, nanocubes, corner-grown nanocubes, and starlike by varying the process conditions, such as the concentration of precursors, heating rate, and the aging time.

Experimental Section

Materials. The synthesis of the ferrite nanocrystals was carried out using commercially available reagents. All the chemicals, including absolute ethanol, hexane, oleic acid, 1-octadecene (90%), diethylene glycol (maximum limits of impurities), sodium oleate ($CH_3(CH_2)_7CH{=}CH(CH_2)_7COONa$, $C_{18}H_{33}O_2Na$, 95+ %), $FeCl_3$ (99+%), and $CoCl_2$ (97+%) were purchased from Fisher Scientific. All the chemicals were used as-received without any further purification.

Chemical Safety and Hazards. As per the information from the Material Safety Data Sheets (MSDS): 1-octadecene may cause eye and skin irritation, and cause respiratory and digestive tract irritation. The toxicological properties of this material have yet to be fully investigated. Oleic acid causes eye, skin, and respiratory tract irritation. Sodium oleate has little or no health hazards. All the reported experimental procedures were carried out in a fume hood with appropriate handling of the chemicals.

Synthesis of Metal Oleate Complexes. The mixed-metal ($Co^{2+}Fe_2^{3+}$)−oleate complex was prepared by reaction of sodium oleate and a mixture of Fe^{3+} and Co^{2+} chlorides. In a typical synthesis, 4 mmol of $FeCl_3$, 2 mmol of $CoCl_2$, 16 mmol of sodium oleate ($C_{18}H_{33}O_2Na$), 10 mL of H_2O, 10 mL of ethanol, and 20 mL of hexane were mixed and refluxed at 60 °C for 4 h. The mixed $Co^{2+}Fe_2^{3+}$−oleate complex ($CoFe_2(C_{18}H_{33}O_2)_8$) was obtained by separation of the water phase and subsequent evaporation of the residual ethanol and hexane at 70 °C and water at 110 °C.

Formation Mechanism of Monodisperse $CoFe_2O_4$ Nanocrystals. Five grams of the mixed-metal ($Co^{2+}Fe_2^{3+}$)−oleate complex, 20 mL 1-octadecene, and 0.5 g oleic acid were mixed and magnetically stirred for 1 h under flowing N_2. The mixture was then heated to 320 °C at a heating rate of 10 °C/min and maintained at this temperature for 120 min under N_2 flow with continuous stirring. A small amount of the sample was withdrawn intermittently from the reaction solution at 200, 250, 280, 305, and 314 °C during heating, and at 320 °C after aging for 0, 5, 10, 30, 60, and 120 min for TEM imaging and magnetic property measurement of the products.

Synthesis of Shape-Controlled Monodisperse $CoFe_2O_4$ Nanocrystals. *(a) Spherical Nanocrystals.* Five grams of the mixedmetal ($Co^{2+}Fe_2^{3+}$)−oleate complex, 20 mL of 1-octadecene, and 0.5 g of oleic acid were mixed and magnetically stirred for 1 h under flowing N_2. The mixture was then heated to 310 °C at a heating rate of 1 °C/min and maintained at this temperature for 60 min under N_2 flow with continuous stirring. The reaction mixture was subsequently cooled to room temperature and transferred to a 50 mL centrifuge tube together with a 20 mL mixture of ethonal and hexane, with a volume ratio of 1:3. Nanocrystals in the form of a black powder was obtained by centrifugation at 8000 rpm for 15 min, which was then dispersed in hexane for storage.

(15) (a) Sun, S; Zeng, H. *J. Am. Chem. Soc.* **2002**, *124*, 8204. (b) Zeng, H.; Rice, P. M.; Wang, S. X.; Sun, S. *J. Am. Chem. Soc.* **2004**, *126*, 11458. (c) Cross, W. B.; Affleck, L.; Kuznetsov, M. V.; Parkin, I. P.; Pankhurst, Q. A. *J. Mater. Chem.* **1999**, *9*, 2545.
(16) (a) Chinnasamy, C. N.; Jeyadevan, B.; Shinoda, K.; Tohji, K.; Djayaprawira, D. J.; Takahashi, M.; Joseyphus, R. J.; Narayanasamy, A. *Appl. Phys. Lett.* **2003**, *83*, 2862. (b) Bao, N.; Shen, L.; Padhan, P.; Gupta, A. *Appl. Phys. Lett.* **2008**, *92*, 173101. (c) Salazar-Alvarez, G.; Qin, J.; Sepelak, V.; Bergmann, I.; Vasilakaki, M.; Trohidou, K. N.; Ardisson, J. D.; Macedo, W. A. A.; Mikhaylova, M.; Muhammed, M.; Baro, M. D.; Nogues, J. *J. Am. Chem. Soc.* **2008**, *130*, 13234.
(17) (a) Shafi, K. V. P. M.; Gedanken, A.; Prozorov, R.; Balogh, J. *Chem. Mater.* **1998**, *10*, 3445. (b) Lu, A. H.; Salabas, E. L.; Schuth, F. *Angew. Chem., Int. Ed.* **2007**, *46*, 1222. (c) Liu, C.; Zou, B.; Rondinone, A. J.; Zhang, Z. J. *J. Am. Chem. Soc.* **2000**, *122*, 6263. (d) Deng, Y.; Qi, D.; Deng, C.; Zhang, X.; Zhao, D. *J. Am. Chem. Soc.* **2008**, *130*, 28. (e) Xu, X.; Friedman, G.; Humfeld, K. D.; Majetich, S. A.; Asher, S. A. *Chem. Mater.* **2002**, *14*, 1249. (f) Ge, J.; Hu, Y.; Yin, Y. *Angew. Chem., Int. Ed.* **2007**, *46*, 1. (g) Ge, J.; Hu, Y.; Biasini, M.; Beyermann, W. P.; Yin, Y. *Angew. Chem., Int. Ed.* **2007**, *46*, 4342. (h) Ge, J.; Hu, Y.; Zhang, T.; Yin, Y. *J. Am. Chem. Soc.* **2007**, *129*, 8974.
(18) (a) Jun, Y. W.; Seo, J. W.; Cheon, J. *Acc. Chem. Res.* **2008**, *41*, 179. (b) Kim, J.; Kim, H. S.; Lee, N.; Kim, T.; Kim, H.; Yu, T.; Song, I. C.; Moon, W. K.; Hyeon, T. *Angew. Chem., Int. Ed.* **2008**, *47*, 8438. (c) Lee, I. S.; Lee, N.; Lee, J. S.; Lee, N.; Park, J.; Kim, B. H.; Yi, Y. W.; Kim, T.; Kim, T. K.; Lee, I. H.; Paik, S. R.; Hyeon, T. *J. Am. Chem. Soc.* **2006**, *128*, 10658. (d) Gu, H.; Xu, K.; Xu, C.; Xu, B. *Chem. Commun.* **2006**, 941.
(19) Song, Q.; Zhang, Z. J. *J. Am. Chem. Soc.* **2004**, *126*, 6164.

(b) Cubic Nanocrystals. Five grams of the mixed metal ($Co^{2+}Fe_2^{3+}$)−oleate complex, 20 mL of 1-octadecene, and 0.5 g of oleic acid were mixed and magnetically stirred for 1 h under flowing N_2. The mixture was then heated to 320 °C at a rate of 1 °C/min and maintained at this temperature for 120 min under N_2 flow with continuous stirring. The follow-up procedures were the same as described in the synthesis of spherical particles, with a black dispersion of cubic nanocrystals obtained in hexane.

(c) Corner-Grown Cubic Nanocrystals. Three grams of the mixed metal ($Co^{2+}Fe_2^{3+}$)−oleate complex, 20 mL of 1-octadecene, and 0.5 g of oleic acid were mixed and magnetically stirred for 1 h under flowing N_2. The mixture was then heated to 300 °C at a heating rate of 0.7 °C/min and maintained at this temperature for 150 min under N_2 flow with continuous stirring. The follow-up procedures were the same as described in the synthesis of spherical particles, with a black dispersion of corner-grown cubic nanocrystals obtained in hexane.

(d) Starlike Nanocrystals. Five grams of the mixed metal ($Co^{2+}Fe_2^{3+}$)−oleate complex, 20 mL of 1-octadecene, and 0.5 g of oleic acid were mixed and magnetically stirred for 1 h under flowing N_2. The mixture was then heated to 320 °C at a heating rate of 5 °C/min and maintained at this temperature for 120 min, under N_2 flow with continuous stirring. The follow-up procedures were the same as described in the synthesis of spherical particles, with a black dispersion of starlike nanocrystals obtained in hexane.

Characterization of Materials. The morphology and structure of the products were characterized using transmission electron microscopy (TEM) coupled with high-resolution (HR) (Tecnai F-20). thermogravimetric analysis (TGA; Model TGA 2950, TA Instrument, Inc., New Castle, DE) was performed on 20 mg of the individual and mixed $Co^{2+}Fe_2^{3+}$−oleate complexes in aluminum sample pans at a heating rate of 5 °C/min up to 600 °C in air. Alternating gradient magnetometry (AGM) was used to measure the magnetic properties of the samples drawn from the reaction mixture at 200, 250, 280, 305, 314, and 320 °C during the heating cycle. A 0.1 mL of the hexane (0.5 mL)-diluted reaction solution (0.1 mL) was dried on a 1.5×1.5 mm^2 Si wafer for the magnetic measurements.

Computational Details. The optimal structure of the cobalt oleate ($Co(CH_3(CH_2)_7CH{=}CH(CH_2)_7COO)_2$) and iron oleate ($Fe(CH_3(CH_2)_7CH{=}CH(CH_2)_7COO)_3$) complexes were determined based on theoretical calculations. All the calculations were performed using the Gaussian 03, Revision E.01 package.[21] The geometrical optimization of the Fe− and Co−oleate complex were performed using all-electron density-functional theory (DFT) with the popular B3LYP (Becke, three-parameter, Lee−Yang−Parr) method,[22] hybrid exchange-correlation functional and 6-31G(d) basis set.[23] The diffuse functions were applied to metals and O in carboxyl group only, in which electron lone pairs play a key role in the formation of coordination bonds. The binding energy (BE) reported in this study is defined as $BE = [(E_{M\text{-complex}} - (E_M{}^{n+} + NE_{oleic\ acid})]/N$, where, E is the total energy and *N* is the coordination number. Hence, negative (positive) BE denotes an exothermic (endothermic) binding process. The charge (*q*) transferred from ligands to metal cations is calculated as Mulliken atomic charge per ligand.

Results and Discussion

Formation Mechanism of Thermolysis Synthesis of $CoFe_2O_4$ Nanocrystals. Since the first report by Hyeon's group on the synthesis of monodisperse nanocrystals using inexpensive and nontoxic iron−oleate complex as a reactant,[24] the method has been utilized for the synthesis of many other binary metal oxides.[25] However, the synthesis of ternary compounds using metal−oleate complexes has thus far been limited to copper−indium sulfide nanocrystal heterostructures.[26] In this case, the segregation of Cu_2S and In_2S_3 leads to the formation of unique heterostructures of various shapes. This behavior is likely due to the differences in the decomposition temperature of the Cu and In−oleate precursors. We recently reported on the synthesis of monodisperse nanocrystals of a number of spinel ferrites with uniform composition via thermolysis of mixed binary metal−oleate precursors. The choice of an intimately mixed precursor, with a decomposition temperature similar to that of the constituent oleates, is critical for the compositional and structural uniformity of the ternary nanocrystals. Here, we have investigated in detail the formation mechanism of the monodisperse $CoFe_2O_4$ nanocrystals from the thermal-decomposition of the metal oleate complexes.

As shown in Figure 1a, carboxylate groups can interact with metal cations in four different configurations, namely, ionic (Figure 1a-*a*), unidentate (Figure 1a-*b*), bidentate (Figure 1a-*c*), and bridging (Figure 1 a-*d*).[27] For the ionic type (Figure 1a-*a*), which is commonly observed in the alkali metal salts of carboxylic acids, the two oxygen atoms in the carboxylate group are equally associated with the metal cation, thus providing the carboxylate ion with a symmetrical structure. For the unidentate carboxylate configuration (Figure 1a-*b*), the symmetry of the functional group is lower because only

(20) Bao, N.; Shen, L.; Padhan, P.; Gupta, A. *J. Am. Chem. Soc.* **2007**, *129*, 12374.
(21) Frisch, J.; , et al. Gaussian 03, revision E.01, Gaussian, Inc.: Wallingford, CT, 2004.
(22) (a) Lee, C.; Yang, W.; Parr, R. G. *Phys. Rev. B* **1988**, *37*, 785. (b) Becke, A. D. *J. Chem. Phys.* **1993**, *98*, 5648.
(23) (a) Ditchfield, R.; Hehre, W. J.; Pople, J. A. *J. Chem. Phys.* **1971**, *54*, 724. (b) Rassolov, V. A.; Ratner, M. A.; Pople, J. A.; Redfern, P. C.; Curtiss, L. A. *J. Comput. Chem.* **2001**, *22*, 976.
(24) (a) Park, J.; An, K.; Hwang, Y.; Park, J. G.; Noh, H. J.; Kim, J. Y.; Park, J. H.; Hwang, N. M.; Hyeon, T. *Nat. Mater.* **2004**, *3*, 891. (b) Choi, S. H.; Kim, E. K.; Park, J.; An, K.; Lee, N.; Kim, S.; Hyeon, T. *J. Phys. Chem. B* **2005**, *109*, 14792. (c) An, K.; Lee, N.; Park, J.; Kim, S. C.; Hwang, Y.; Park, J. G.; Kim, J. Y.; Park, J. H.; Han, M. J.; Yu, J.; Hyeon, T. *J. Am. Chem. Soc.* **2006**, *128*, 9753. (d) Yu, T.; Park, J.; Moon, J.; An, K.; Piao, Y.; Hyeon, T. *J. Am. Chem. Soc.* **2007**, *129*, 14558. (e) Kwon, S. G.; Piao, Y.; Park, J.; Angappane, S.; Jo, Y. N.; Hwang, M.; Park, J. G.; Hyeon, T. *J. Am. Chem. Soc.* **2007**, *129*, 12571. (f) Yu, W. W.; Falkner, J. C.; Yavuz, C. T.; Colvin, V. L. *Chem. Commun.* **2004**, 2306.
(25) (a) Gu, H.; Soucek, M. D. *Chem. Mater.* **2007**, *19*, 1103. (b) Zhang, Y.; Zhu, J.; Song, X.; Zhong, X. *J. Phys. Chem. C* **2008**, *112*, 5322. (c) Lee, D. K.; Kim, Y. H.; Kang, Y. S.; Stroeve, P. *J. Phys. Chem. B* **2005**, *109*, 14939. (d) Han, Y. C.; Cha, H. G.; Kim, C. W.; Kim, Y. H.; Kang, Y. S. *J. Phys. Chem. C* **2007**, *111*, 6275. (e) Han, M.; Liu, Q.; He, J.; Song, Y.; Xu, Z.; Zhu, J. *Adv. Mater.* **2007**, *19*, 1096. (f) Buonsanti, R.; Grillo, V.; Carlino, E.; Giannini, C.; Curri, M. L.; Innocenti, C.; Sangregorio, C.; Achterhold, K.; Parak, F. G.; Agostiano, A.; Cozzoli, P. D. *J. Am. Chem. Soc.* **2006**, *128*, 16953.
(26) Chio, S. H.; Kim, E. G.; Hyeon, T. *J. Am. Chem. Soc.* **2006**, *128*, 2520.
(27) (a) Mehrotra, R. C.; and Bohra, R. In Metal Carboxylates; Academic Press: New York, 1983; Chapter 3. (b) Einspahr, H.; Bugg, C. Acta Crystallogr., Sect. B 1980, 36, 1044. (c) Lu, Y.; Miller, J. D. J. Colloid Interface Sci. 2002, 256, 41.

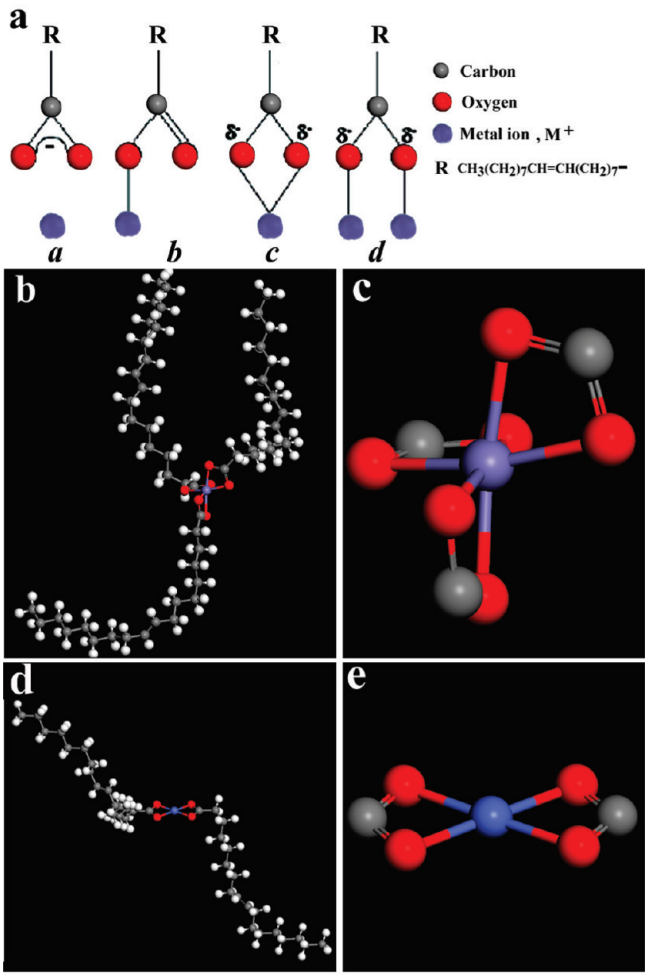

Figure 1. (a) Four coordination modes: (*a*) ionic, (*b*) unidentate, (*c*) bidentate, and (*d*) bridging, for the interaction between carboxylate groups and metal cations. (b) Full view and (c) central core of the optimized iron oleate ($Fe(CH_3(CH_2)_7CH{=}CH(CH_2)_7COO)_3$) complex structure. (d) Full view and (e) central core of the optimized cobalt oleate ($Co(CH_3(CH_2)_7CH{=}CH(CH_2)_7COO)_2$) complex structure.

one oxygen atom is coordinated with the metal cation. The carboxylate group in the bidentate mode (Figure 1a-*c*) has the same group symmetry as in the free ionic state (Figure 1a-*a*). Finally, in the bridging coordination (Figure 1a-*d*), only one oxygen coordinates with a particular cation. Therefore, the bridging mode is similar to the unidentate coordination (Figure 1a-*b*). However, the group symmetry is similar to that in the bidentate coordination.

The coordination characteristics of the metal ions determine the nature of the metal carboxylate salts. The Co^{2+} and Fe^{3+} ions in the ($Co^{2+}Fe_2^{3+}$)−oleate complex used for thermolysis synthesis of $CoFe_2O_4$ coordinate only oxygen atoms from carboxylate groups, because solvent molecules such as water and ethanol containing oxygen and hydroxyl groups are removed. This is different from a previously reported synthesis carried out in the presence of oxygen-containing solvent molecules, such as water and ethanol. For charge balance, each Co^{2+} [28] and Fe^{3+} ion combines with two and three oleate ion groups ($CH_3(CH_2)_7CH{=}CH(CH_2)_7COO^-$), respectively, to form the complexes. Co^{2+} and Fe^{3+} coordinate four and six oxygen from the carboxylate groups in the respective complex, satisfying the unidentate (Figure 1a-*b*) or bidentate (Figure 1a-*c*) metal carboxylate coordination modes. One expects the bidentate mode (Figure 1a-*c*) to be favored, because it has higher group symmetry and a lower energy. We performed theoretical calculations to determine the optimal cobalt− and iron−oleate complex structures.

Figure 1 shows the optimized complex structures for the iron oleate ($Fe(CH_3(CH_2)_7CH{=}CH(CH_2)_7COO)_3$) (panels b and c in Figure 1) and cobalt oleate ($Co(CH_3(CH_2)_7CH{=}CH(CH_2)_7COO)_2$) (panels d and e in Figure 1). As seen in Figure 1b, two of the three oleate ligands bound to the iron are closer because of van der Waals attraction. The third one is located on the opposite side and does not interact with the remaining two oleate ligands. Each of the three oleate ligands bind to iron through an Fe−O coordination bond. Totally, one Fe^{3+} coordinates six oxygen atoms of the carboxylate groups from three oleate ligands to form an octahedral structure with 17 electron species (Figure 1c). The entire iron oleate complex molecule has an asymmetric structure (Figure 1b), but the Fe−O coordination has a structure of D_3 symmetry (Figure 1c). The calculated binding energy for $Fe(CH_3(CH_2)_7CH{=}CH(CH_2)_7COO)_3$ is −18.90 eV, lower than that of −12.20 eV for $Fe(CH_3(CH_2)_7CH{=}CH(CH_2)_7COO)_2^+$ formed by releasing the third oleate ligand from the $Fe(CH_3(CH_2)_7CH{=}CH(CH_2)_7COO)_3$. As compared with the structure of the iron oleate complex (Figure 1b), the cobalt oleate complex molecule has a symmetric structure (Figure 1d). As seen in Figure 1d, the two oleate ligands bound to the cobalt are equivalent and are located in opposite positions for maintaining the lowest energy. One Co^{2+} coordinates four oxygen atoms of the carboxylate groups from two oleate ligands to form a symmetrically planar D_{2h} structure (Figure 1 d). The calculated binding energy for the cobalt oleate is −13.30 eV. The charge (q) transferred from ligands to metal cations is 1.08, 0.88, and 0.83 electron/per ligand for $Fe(CH_3(CH_2)_7CH{=}CH(CH_2)_7COO)_3$, $Fe(CH_3(CH_2)_7CH{=}CH(CH_2)_7COO)_2^+$, and $Co(CH_3(CH_2)_7CH{=}CH(CH_2)_7COO)_2$ complexes, respectively, showing very close metal cation−oleate bond strength for these three compounds.

Figure 2 shows the TGA curves of the individual Fe^{3+}−oleate (Figure 2a-a) and Co^{2+}−oleate (Figure 2a-b) complex, and the mixed ($Co^{2+}Fe_2^{3+}$)−oleate complex (Figure 2a-c). Three different weight-loss rates are observed in the TGA curve (Figure 2a-a) of the Fe^{3+}−oleate complex. The first, appearing at 200−250 °C, is attributed to the dissociation of a single oleate ligand from the Fe^{3+}−oleate by CO_2 elimination and the formation of a metastable nuclei, and the third one appearing at 300−350 °C results from dissociation of the remaining two oleate ligands to form the final product. The differences in the interaction and structure of three oleate ligands, as seen in Figure 1b, results in the stepwise breakdown of the three ligands. In addition, the first and third

(28) Bronstein, L. M.; Huang, X.; Retrum, J.; Schmucker, A.; Pink, M.; Stein, B. D.; Dragnea, B. *Chem. Mater.* **2007**, *19*, 3624.

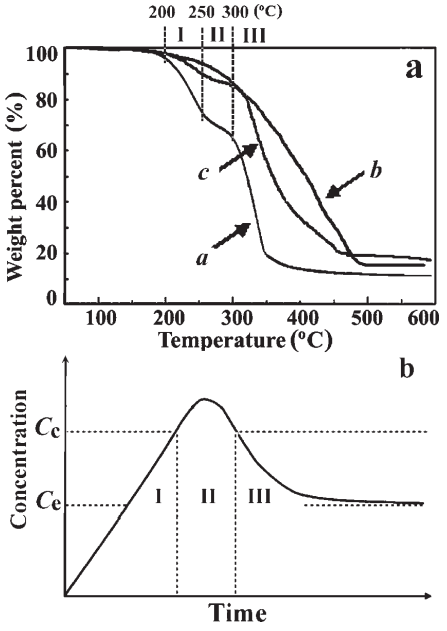

Figure 2. (a) TGA curves of (*a*) Fe−oleate complex, (*b*) Co−oleate complex, and (*c*) the intimately mixed binary $Co^{2+}Fe_2^{3+}$−oleate complex. (b) The LaMer model for the formation of monodisperse nanoparticle. C_c and C_e are the critical nucleation concentration and the equilibrium concentration of the solid products, respectively. I, II, and III represent the prenucleation stage, nucleation stage, and growth stage of the nanoparticle products, respectively.

weight losses observed in the TGA are separated by a continuous slow weight loss covering the temperature range of 250−300 °C, which is caused by the dissociation of either the free or weakly bound oleate molecules to the iron.[24a,28] The break between the first and third weight losses by about 50 °C is important for the synthesis of monodisperse nanoparticles, because it helps separate the nucleation and growth processes.[29] In contrast, because the cobalt oleate complex has a symmetric structure (panels d and e in Figure 1) and the strength of two oleate bonds in the Co^{2+}−oleate complex are comparable, a continuous weight loss is observed for this complex in the temperature range of 200−500 °C (Figure 1a-b). The TGA curve (Figure 1a-c) of the well-mixed ($Co^{2+}Fe_2^{3+}$)−oleate complex exhibits a weight loss behavior similar to that of the pure Fe^{3+}−oleate complex, but with a much smaller weight loss in the temperature range of 200−300 °C. The rapid weight loss for the mixed complex commences at 300−320 °C.

LaMer et al. have described the formation mechanism of monodisperse nanocrystals by separating the nucleation and the growth steps in the homogeneous nucleation process, as shown in Figure 2b[1,30] In general, nonseeded growth of monodisperse nanocrystals by thermal decomposition of metallorganic synthetic precursors is consistent with this formation mechanism. The monomer concentration builds up in the prenucleation stage (stage I in Figure 2b) from decomposition of the precursor. However, even when the accumulated concentration of the monomers is above the equilibrium concentration (C_e in Figure 2b), precipitation of nanocrystals does not occur because of the unfavorable supersaturation condition. The monomer concentration continues to increase with time until it reaches a critical nucleation concentration (C_c in Figure 2b), at which point initial nucleation of the nanocrystals (stage II in Figure 2b) takes place. During this period, the monomer concentration continues to increase to a maximum and then drops gradually as more and more of the monomers aggregate onto the nuclei. When the monomer concentration in stage II drops below C_c, the system enters the growth stage (stage III in Figure 2b). The product nuclei formed in stage II continue to grow in stage III by incorporating additional monomers until their concentration drops to C_e.

We have qualitatively monitored the progress of the reaction as a function of temperature by measuring the magnetic moment of the reaction product at various stages of the thermolysis of both the Fe^{3+}−oleate and the mixed ($Co^{2+}Fe_2^{3+}$)−oleate complexes. The magnetic moment of a 0.1 mL hexane-diluted solution, drawn at 200, 250, 280, 305, and 314, and 320 °C during the heating cycle, has been measured after drying the solution on a Si wafer. For the synthesis of monodisperse Fe_2O_3 nanocrystals by thermal decomposition of the pure Fe^{3+}−oleate complex, a very small magnetic moment is measured at 200−250 °C. A gradual increase in the magnetic moment occurs for the product formed in the temperature range of 250−300 °C, followed by a much more rapid increase for $T > 300$ °C. The very small magnetic moment for the 200−250 °C sample indicates that the Fe_2O_3 nuclei begin to form in the reaction solution at these temperatures, but are unstable and can readily dissolve. Although the monomer concentration is higher than the equilibrium concentration (C_e in Figure 2b), corresponding to the solubility of bulk solid Fe_2O_3, spontaneous homogeneous nucleation does not occur because of the high activation barrier when the monomer concentration is below the critical concentration (C_c in Figure 2b) for nucleation. With increasing the temperature to 250−300 °C, the monomer concentration increases continuously, but few Fe_2O_3 nuclei are produced until the monomer concentration reaches the critical concentration (C_c in Figure 2b). At around 300 °C, the monomer concentration is higher than the critical concentration, and the supersaturation is sufficiently high to overcome the energy barrier for spontaneous homogeneous. Thereafter, fast nucleation of the nanocrystals occurs closely associated with the rapid decomposition of the Fe^{3+}−oleate complex. Similarly, for the thermolysis of the well-mixed ($Co^{2+}Fe_2^{3+}$)−oleate complex, the magnetic moment of the reaction product shows a similar tendency with increasing temperature, but the measured magnetic moment is significantly higher. We thus conclude that the initial formation of $CoFe_2O_4$ nuclei occurs at 200−250 °C, and the monomer concentration increases in the temperature range of 250−300 °C. A rapid increase in the monomer concentration occurs for temperatures above 300 °C because of the fast dissociation of the precursor, resulting in increased nucleation of the $CoFe_2O_4$ nanocrystals.

(29) Talapin, D. V.; Shevchenko, E. V.; Weller, H. Synthesis and Characterization of Magnetic Nanoparticles. In Nanoparticles; Schmid, G., Ed.; Wiley-VCH: Weinheim, Germany, 2004.
(30) LaMera, V. K.; Dinegar, B. H. *J. Am. Chem. Soc.* **1950**, *72*, 4847.

We have made extensive use of transmission electron microscopy (TEM) to investigate the formation and shape evolution of $CoFe_2O_4$ nanocrystals. A small aliquot of the solution is rapidly withdrawn from the reaction mixture during the heating cycle for analysis of the solid product when the temperature reaches 250, 280, 305, 314, and 320 °C. Additionally, we have analyzed the product formed at 320 °C after being maintained at this temperature for 5, 10, 30, 60, and 120 min. TEM observation of samples withdrawn below 300 °C without any aging do not show any evidence of product formation. This is consistent with our earlier conclusion that the monomer concentration at these temperatures is lower than the critical concentration. Although some $CoFe_2O_4$ nuclei, consisting of only a few crystal units, may appear at this stage, it is difficult to observe them. However, as seen in Figure 3, product samples analyzed above 300 °C reveal definite formation of monodisperse nanocrystals of different shapes and sizes depending on the reaction temperature and aging time. The sample taken at 305 °C provides evidence of the early stage of nanocrystal formation. As seen in Figure 3a, very small monodisperse nuclei, with a uniform size of less than 2 nm, are formed through spontaneous homogeneous nucleation when the accumulated monomer concentration increases rapidly above the critical concentration at $T > 300$ °C. With further increasing the reaction temperature to 314 °C in less than 1 min, the $CoFe_2O_4$ nuclei grow fast to form monodisperse spherical nanocrystals with a uniform size of 8.3 ± 0.3 nm, as seen in Figure 3b and the Supporting Information, SI1. As the reaction temperature is further increased to 320 °C in another 35 s, the spherical nanocrystals continue to grow to form nanocubes with rounded corners (Figure 3c and the Supporting Information, SI2), indicating a spherical-to-cubic shape evolution for the products. The size of the nanocrystals at this stage is about 8.5 ± 0.4 nm, which is somewhat larger than those synthesized at 314 °C. On the basis of these results, we conclude that the homogeneous nucleation of $CoFe_2O_4$ nanocrystals occurs at 300−314 °C and is essentially complete within 1 min. This is consistent with the LaMer mechanism and the results obtained from magnetic measurements. With prolonging the dwell (aging) time at 320 °C to 5, 10, 30, 60, and 120 min, more and more of the spherical nanocrystals continue growing to form nanocubes, but at a reduced growth rate, as can be seen by comparing the images in Figure 3d−g. After the longest aging period (120 min), the product almost completely transforms into nanocubes with a high yield and narrow size distribution (Figure 3h). All the synthesized products readily form suspensions in hexane that then produce well-ordered superlattices over large areas after slow evaporation of the solvent (see the Supporting Information, SI1−7).

Additional details regarding the average size, distribution, and percentage of different shape nanocrystals formed at 320 °C, after being aged for 0−120 min, is provided in Figures 4a, 4b, and 5, respectively. As seen in Figure 4a, the average size of the $CoFe_2O_4$ nanocrystals increases rapidly from 8.3 ± 0.3 nm for 314 °C without any aging to 10.1 ± 0.3 nm for 320 °C with 10 min of aging. With further increase in the aging time at this temperature to 60 min, the average size slowly increases to 11.2 nm, and then appears to level off at about 11.5 nm after aging for 120 min. As seen from the histograms in Figure 4b, the size distribution of the product synthesized at 320 °C narrows with increasing aging time from 0 to 30 min, and is then stable for longer periods (60−120 °C). Figure 5 shows the percentage of spherical, spherical-to-cubic, and cubic shaped products synthesized at 320 °C after aging for 0−120 min. The shape evolution with increasing aging time from spherical, to the intermediate spherical-to-cubic, and eventually to cubic morphology is apparent in Figure 5.

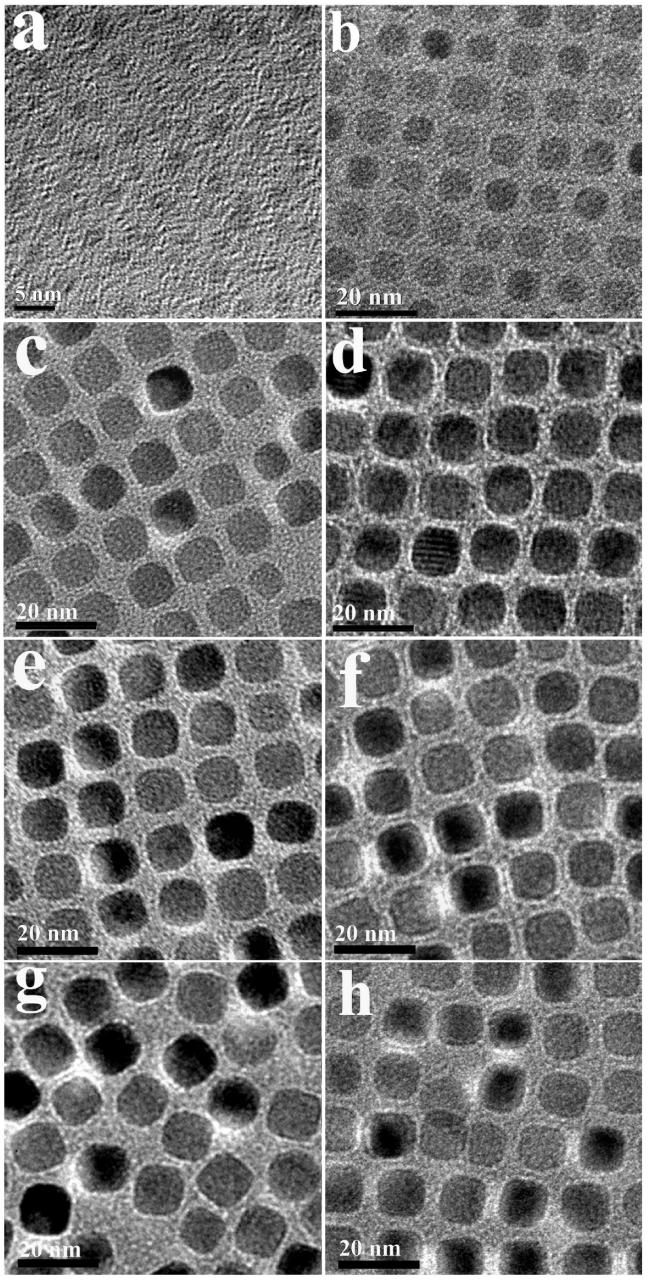

Figure 3. TEM images of the $CoFe_2O_4$ nanocrystals sampled from the reaction solution without any aging at (a) 305 and (b) 314 °C, and at 320 °C after aging for (c) 0, (d) 5, (e) 10, (f) 30, (g) 60, and (h) 120 min.

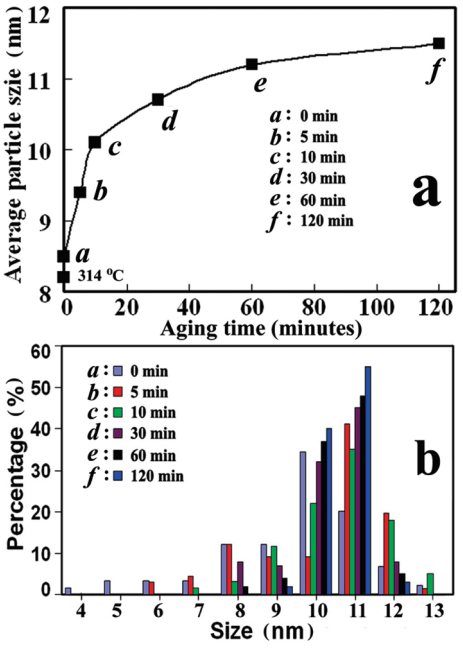

Figure 4. (a) Average particle sizes, and (b) the size distributions of the $CoFe_2O_4$ nanocrystals prepared at 320 °C after aging for (*a*) 0, (*b*) 5, (*c*) 10, (*d*) 30, (*e*) 60, and (*f*) 120 min. The average particle size of the $CoFe_2O_4$ nanocrystals prepared at 314 °C without any aging is also shown.

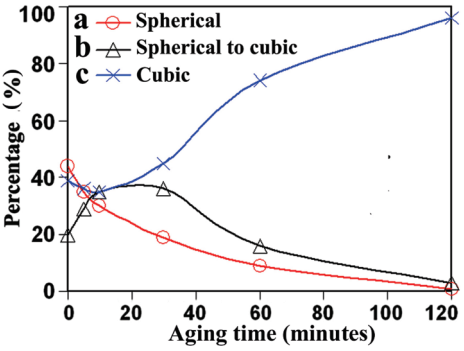

Figure 5. Percentages of $CoFe_2O_4$ nanocrystals with (a) spherical, (b) spherical-to-cubic, and (c) cubic shapes obtained at 320 °C after aging for 0, 5, 10, 30, 60, and 120 min.

On the basis of the results shown in Figures 4 and 5, we infer that both thermodynamic and kinetic factors dictate the size and shape evolution of the $CoFe_2O_4$ nanocrystals at different stages of the reaction, with the organic surfactant also playing an important role. Below 314 °C, the nanocrystals have a spherical shape with the average size steadily increasing with increasing reaction temperature. With a relatively low monomer concentration, the monomers attach and grow isotropically from the nucleating seeds at a slow growth rate with no specificity in the growth direction, leading to the thermodynamically favored spherical morphology. Under these conditions, the surface energy contribution primarily determines the shape and size of the nanocrystals, because the spherical shape has the lowest surface area.

With increasing the temperature from 314 to 320 °C and aging at 320 °C for 10 min, results in a rapid increase in the average size (Figure 4a), with a broader size distribution (Figure 4b), and with roughly equal amounts of the different shape (spherical, spherical-to-cubic, and cubic) nanocrystals (Figure 5). This indicates that the equilibrium crystal structure with minimum surface energy increasingly dominates the shape of the $CoFe_2O_4$ nanocrystals with increasing monomer concentration. The intermediate spherical-to-cubic shape nanocrystals are faceted with both the {100} and {111} faces of the fcc structure exposed. Because the surface energy of the {111} faces is higher than that of the {100} faces,[31] relatively fast growth along the ⟨111⟩ directions results in the eventual formation of cube-shaped nanocrystals with {100} facets, which has also been observed for synthesis of other magnetic nanocrystals.[32]

Most of the spherical $CoFe_2O_4$ nanocrystals keep growing to form the cubic shape until the excess monomers in the solution are nearly exhausted and their concentration reduces to C_e (Figure 2b). The controlling parameter dividing the thermodynamic surface-energy and the crystal-shape-controlled growth regimes is the average particle size. The average particle size varies with the reaction conditions, such as the concentration of the precursors, temperature, the values of C_e and C_c, etc. The percent of cubic-shaped nanocrystals increases significantly from 42% to about 95%. The well-known Ostwald ripening occurs at this reaction stage. Because smaller particles have a higher surface free energy due to the Gibbs−Thomson effect,[33] the monomers formed through dissolution of the smaller crystallites lead to the growth of the larger crystals in solution, resulting in a slow increase in their average sizes and a decrease in the size distribution.

Shape-Controlled Monodisperse $CoFe_2O_4$ Nanocrystals. With controlling the nucleation and growth rate by varying the synthesis conditions, the nanocrystals can be tuned in the form of spherical, cubic, corner-grown cubic, and starlike shapes. We have found that the cubic shape is the most stable product, and it evolves from the initial spherical shape formed at the nucleation stage. Therefore, the strategy to synthesize spherical $CoFe_2O_4$ nanocrystals is to induce homogeneous nucleation under as high a supersaturation as possible, and reducing the growth stage in order to avoid the spherical-to-cubic shape transformation. In contrast, relatively higher temperature and longer aging time, as compared with the synthetic condition of the spherical shaped product, are necessary for the growth of cubic shape product. A longer aging time of 120 min at 320 °C results in near-complete transformation to the cubic-shaped product.

Figure 6a−d show the TEM and HRTEM images of spherical (10.6 ± 0.3 nm) and cubic nanocrystals

(31) (a) Davies, M. J.; Parker, S. C.; Watson, G. W. *J. Mater. Chem.* **1994**, *4*, 813. (b) Fang, C. M.; Parker, S. C.; De With, G. *J. Am. Ceram. Soc.* **2000**, *83*, 2082.
(32) (a) Kim, D.; Lee, N.; Park, M.; Kim, B. H.; An, K.; Hyeon, T. *J. Am. Chem. Soc.* **2009**, *131*, 454. (b) Dunin-Borkowski, R. E.; McCartney, M. R.; Frankel, R. B.; Bazylinski, D. A.; Posfai, M.; Buseck, P. R. *Science* **1998**, *282*, 1868. (c) Mann, S.; Frankel, R. B.; Blakemore, R. P. *Nature* **1984**, *310*, 405.
(33) Lifshitz, I. M.; Slyozov, V. V. *J. Phys. Chem. Solids* **1961**, *19*, 35.

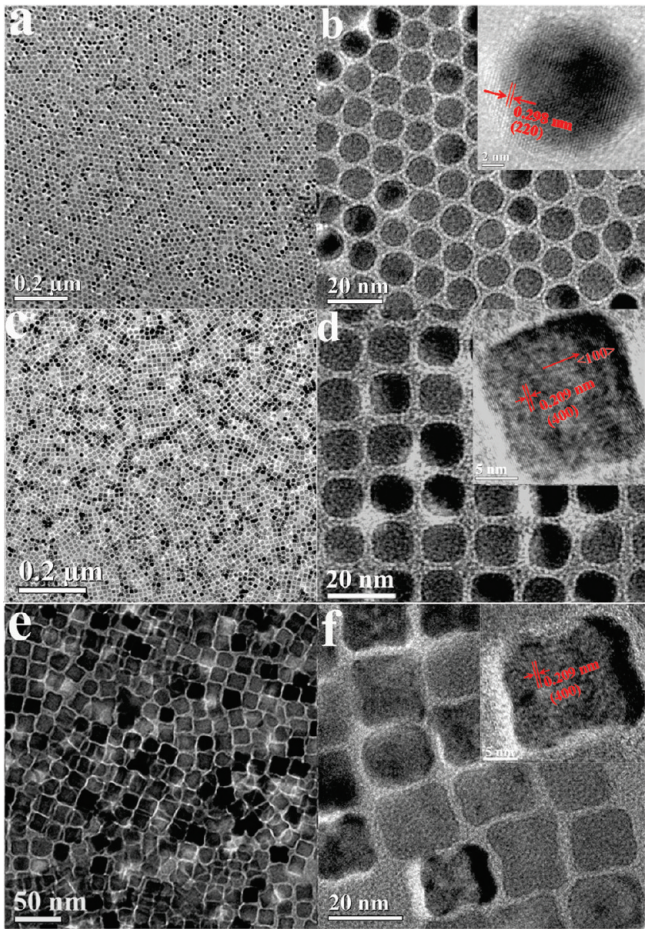

Figure 6. TEM and HRTEM images of (a, b) spherical, (c, d) cubic, and (e, f) corner-grown cubic $CoFe_2O_4$ nanocrystals at different magnifications. (a, c, e) Lower- and (b, d, f) higher-magnification TEM images, showing a very high yield, monodispersity, and uniformity of the synthesized $CoFe_2O_4$ nanocrystals. The insets of b, d, and f show HRTEM images of individual spherical, cubic, and corner-grown cubic nanocrystals, respectively. Clear crystal lattices are observed in the HRTEM images (the insets of b, d, and f), indicating the single-crystalline nature of the nanocrystals.

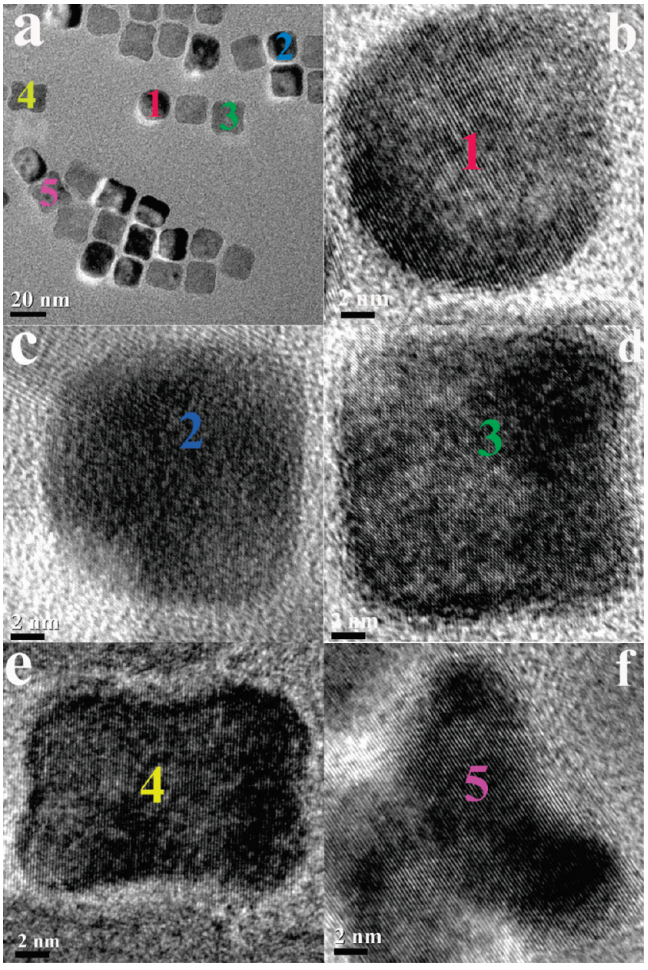

Figure 7. (a–f) TEM and HRTEM images of some intermediate products coexisting with the corner-grown $CoFe_2O_4$ nanocrystals, which indicates a shape evolution from (b) spherical, to (c) spherical-to-cubic, to (d) near-cubic, to (e) corner-grown cubic, and to (f) starlike shaped nanocrystals marked with 1, 2, 3, 4, and 5 in Figure 7a, respectively.

(11.8 ± 0.4 nm). Both types of nanocrystals exhibit a narrow size distribution that forms well-ordered superlattices over large areas after slow evaporation of the solvent (images a and c in Figure 6). The HRTEM images (the insets to b and d in Figure 6) of the various $CoFe_2O_4$ nanocrystals show clear lattice fringes corresponding to a group of atomic planes, confirming their single crystalline nature. The yields of the perfectly spherical and cubic nanocrystals with sharp edges, shown in Figure 6, are essentially 100%.

In contrast to the synthetic conditions of spherical nanocrystals, decreases in the reactant concentration, heating rate, and the reaction temperature are still favorable for supersaturation, but with reduced formation of nanocrystals. However, they can grow as long as there is a continuous source of the monomers available through slow decomposition of the oleate precursor. Because the consumption rate of the momoners for crystal growth rate is higher than their formation rate, a limited number of nuclei can grow to from large nanocubes. The surface energy and the concentration of defects in the individual crystallites decrease in going from the corners, to the edges, to the crystal faces of nanocubes. Thus, the growth preferences with decreasing growth rate for different sections of nanocubes are the corners, the edges, and the faces, respectively. In principle, one can exploit such a growth progression to develop novel corner- and edge-grown shapes from the cubic intermediates, with eventual formation of the intricate starlike shape. Indeed, by adjusting the reaction conditions we have successfully synthesized the expected corner-grown nanocubes and starlike $CoFe_2O_4$ nanocrystals. As shown in Figure 6e and f, novel corner-grown cubic $CoFe_2O_4$ nanocrystals with a relatively larger size of 18.5 ± 0.8 nm can be synthesized. The yield of the corner-grown cubic shape is estimated to be over 50%. The HRTEM image (the inset to Figure 6f) of a typical corner-grown cubic $CoFe_2O_4$ nanocrystal show clear lattice fringes corresponding to a group of atomic planes, indicating the single crystalline nature. In addition to the formation of the primary corner-grown cubic-shaped product, a few spherical (Figure 7b), spherical-to-cubic (Figure 7c), and near-cubic (Figure 7d) shaped nanocrystals marked

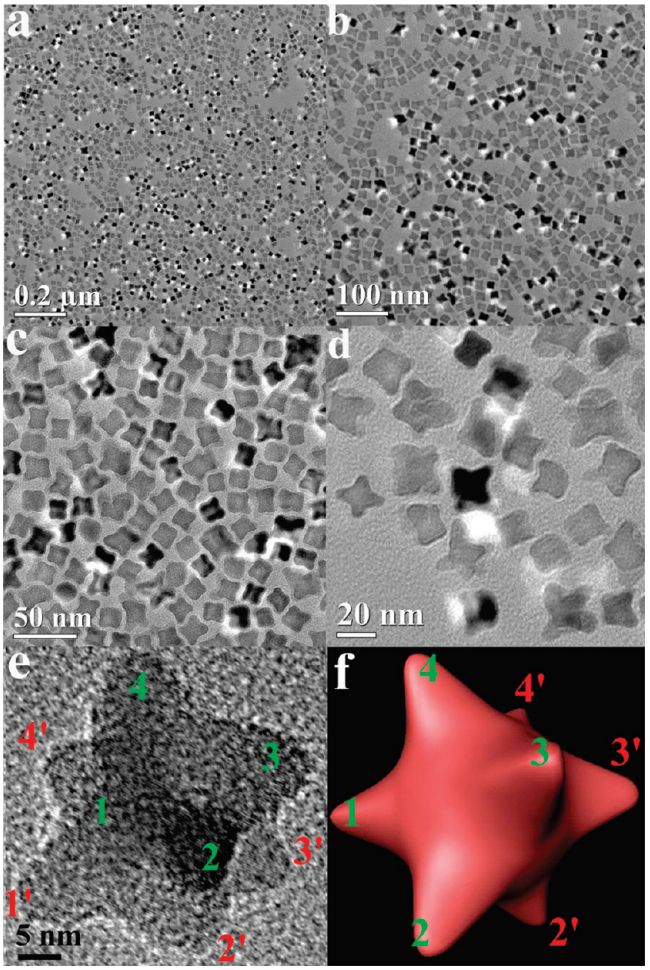

Figure 8. (a–d) TEM images of the starlike $CoFe_2O_4$ nanocrystals at different magnifications. (e) HRTEM image and (f) schematic shape diagram of an individual starlike $CoFe_2O_4$ nanocrystal. The eight sharp horns of the starlike nanocrystal are marked with 1, 1′, 2, 2′, 3, 3′, 4, 4′, respectively.

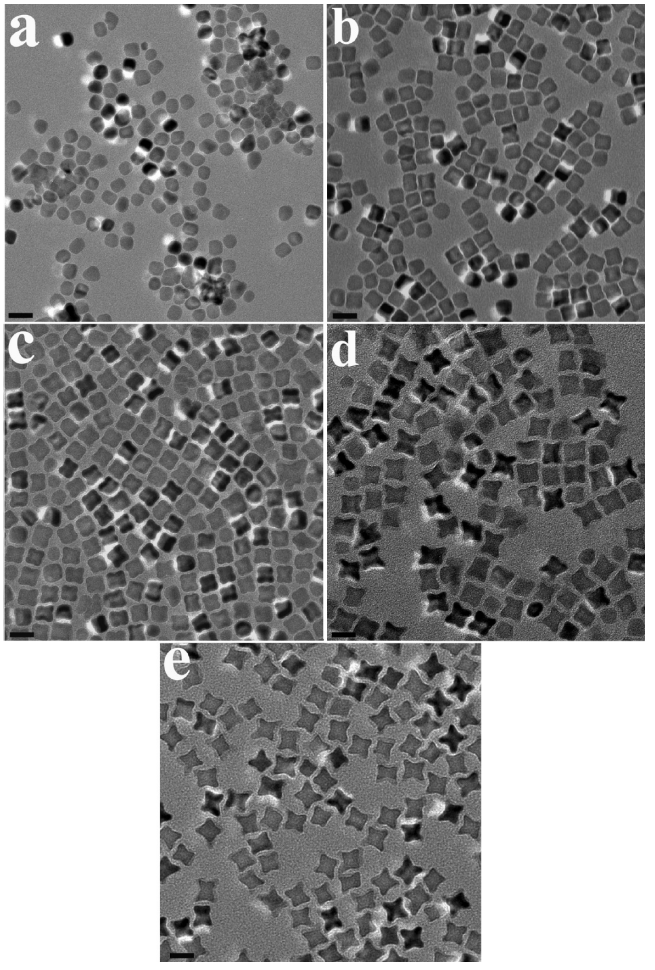

Figure 9. TEM images of the intermediate shapes formed at 320 °C after aging for (a) 0, (b) 10, (c) 30, (d) 60, and (e) 120 min during the formation of the starlike $CoFe_2O_4$ nanocrystals. All the scale bars represent 20 nm.

with 1, 2, and 3 in Figure 7a, respectively, are also observed. The existence of these intermediate-shaped products provides support for the initial formation of spherical nanocrystals with subsequent growth to form mostly the cubic shape nanocrystals, and then to corner-grown nanocubes. Moreover, several starlike nanocrystal products, as seen in Figures 6e and 7f, indicate that the corner-grown nanocubes can be the intermediate-shaped product that further grows to form starlike nanocrystals.

Figure 8 shows the TEM and HRTEM images of novel star-like $CoFe_2O_4$ nanocrystals with a high yield of more than 95% and an average size of 26.6 ± 2.6 nm. The as-prepared nanocrystals readily go into suspension in hexane that then form well-ordered superlattices over large areas after slow evaporation of the solvent, as seen in Figure 8a–d. The HRTEM image (Figure 8e) of an individual star-like nanocrystal shows that the structure consists of eight horns symmetrically distributed around a center core, as illustrated by the schematic diagram (Figure 8f).

We have investigated the shape evolution leading to the formation of the starlike $CoFe_2O_4$ nanocrystals using TEM. As in the earlier studies, a small aliquot of the solution is rapidly withdrawn from the reaction mixture during the heating cycle for analysis of the solid product formed at 320 °C after aging for 0, 10, 30, 60, and 120 min during the formation of the starlike $CoFe_2O_4$ nanocrystals. As seen in Figure 9, product samples analyzed show definite formation of monodisperse nanocrystals with different shapes depending on the aging time. The product formed at 320 °C without aging (Figure 9a) is primarily spherical with a small amount of cubic nanocrystals (<10%). The size of the nanocrystals at this stage is about 11.5 ± 1.4 nm, With prolonging the dwell (aging) time at 320 °C to 10 min, most of the spherical nanocrystals (>80%) continue to grow to form nanocubes (Figure 9b), but some (<20%) still maintain the spherical shape, indicating a spherical-to-cubic shape evolution for the products. The size of the nanocrystals at this stage is about 12.5 ± 1.2 nm, which is larger than the spherical nanocrystals synthesized at 320 °C without aging. These cubic nanocrystals further grow to form corner-grown nanocubes with the size increasing to about 14.2 ± 0.5 nm, as seen from the TEM image of the products formed at 320 °C for 30 min (Figure 9c). The yield of the corner-grown cubic nanocrystals is about 85%, with the

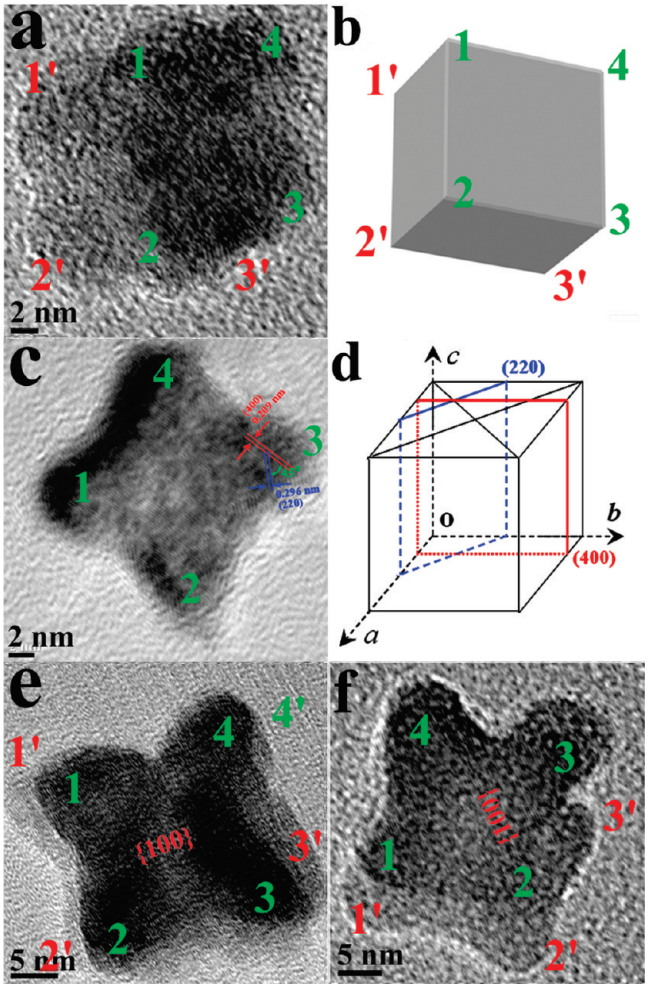

Figure 10. HRTEM images and schematic diagrams of the structures of the intermediate morphologies of the $CoFe_2O_4$ nanocrystals synthesized with increasing the aging time as compared with the synthesis condition of the star-like nanocrystals. (a) HRTEM image and (b) schematic diagram of the initial cubic intermediate. (c) HRTEM image and (d) schematic diagram crystal structure and growth direction of a corner-grown nanocrystal. (e, f) HRTEM images the intermediate shapes between corner-grown nanocube and starlike shape.

remaining being spherical or cubic. With further prolonging the dwell (aging) time at 320 °C to 60 min, the products are mainly starlike nanocrystals except for a small amount (<10%) of spherical and cubic nanocrystals (Figure 9d), indicating that the star-like shape evolves from the corner-grown cubic nanocrystals. After the longest aging period (120 min), almost all the products are starlike nanocrystals (Figure 9e) as the small spherical and cubic nanocrystals dissolve during the final Ostwald-ripening process.

We have further studied the detailed structures of the primary intermediate products as function of aging time at 320 °C. Because we have previously described the spherical-to-cubic shape evolution, we here focus on the cubic-to-star-like shape evolution. As seen in Figure 10, all the intermediate-shape nanocrystals, such as cubic (images a and b Figure 10) and corner-grown nanocube (image c and scheme d in Figure 10), the intermediate

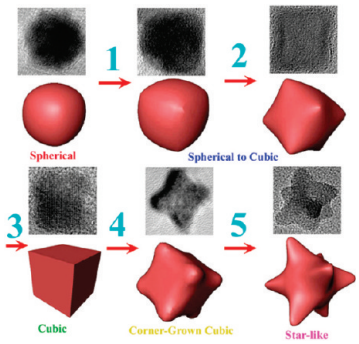

Figure 11. Schematic illustration of the shape evolution mechanism of $CoFe_2O_4$ nanocrystals. (a) spherical, (b, c) spherical-to-cubic, (d) cubic, (e) corner-grown cubic, and (f) star-like.

shape between corner-grown nanocube and starlike shape (images e and f in Figure 10), and starlike shape (image e and scheme f in Figure 8), expose the {100} faces of the fcc structure as the center of side facets. When compared with a perfect fcc-structured ferrite nanocube generally exhibiting only {100} facets, additional {110} facets are observed at the corners or the horn regions of the intermediate-shape nanocrystals, as seen in the HRTEM image (Figure 10b) and crystal-structure schematic diagram (Figure 10c) of a corner-grown nanocube. This indicates that the continuous growth along the eight corners of the intermediate cubic shape results in the formation of the starlike shape. A schematic of the suggested mechanism for the shape evolution of $CoFe_2O_4$ nanocrystals is provided in Figure 11.

Conclusion

In summary, we have studied the formation mechanism of monodisperse ternary $CoFe_2O_4$ nanocrystals by a homogeneous nucleation and growth process utilizing an intimately mixed ($Co^{2+}Fe_2^{3+}$)−oleate complex as synthetic precursor. The close thermal decomposition temperature range of the cobalt and iron oleate complexes is important for the compositional and structural uniformity of the product. Controlling the nucleation and growth dynamics by changing the heating rate, temperature, and the precursor concentration can result in the formation of differently shaped nanocrystals. Because of the inherent cubic symmetry of the spinel structure, the product is largely restricted to isotropic zero-dimensional nanostructures. We believe that the present results are extendible to the synthesis and shape control of a variety of other ternary oxide nanocrystals.

Acknowledgment. This work was supported by NSF under Grant ECS-0621850. Supercomputer resources were provided by the Alabama Supercomputer Center, NCSA TeraGrid, and the Pacific Northwest National Lab EMSL facility.

Supporting Information Available: TEM images (PDF). This material is available free of charge via the Internet at http://pubs.acs.org.